

# Zeolite-Supported Rhodium Complexes and Clusters: Switching Catalytic Selectivity by Controlling Structures of Essentially Molecular Species

Pedro Serna and B. C. Gates\*

Department of Chemical Engineering and Materials Science, University of California, One Shields Avenue, Davis, California 95616, United States

**S** Supporting Information

**ABSTRACT:** Precise synthesis and characterization of site-isolated rhodium complexes and extremely small rhodium clusters supported on zeolite HY allow control of the catalyst selectivity in the conversion of ethene to *n*-butene or ethane, respectively, as a result of tuning the structure of the active sites at a molecular level.

Supported metals are a widely investigated and industrially applied class of catalyst, and their properties are sensitive to subtle changes in structure.<sup>1,2</sup> The structural nonuniformity of most solid catalysts limits the opportunities to control their properties, but when the supported species incorporate only very few metal atoms each, the surface chemistry becomes essentially molecular.<sup>3–6</sup> The supports then take on the role of ligands, providing opportunities to fine-tune the catalytic properties that may rival those in organometallic solution catalysis.<sup>7–9</sup> Furthermore, when the metals are highly dispersed on a support, the opportunities for involving the support in the catalysis are optimized.<sup>10,11</sup>

Here we report how to tune the catalytic properties of small, nearly uniform clusters and site-isolated complexes of rhodium on a highly uniform (crystalline) support, zeolite HY, for control of the selectivity for alkene dimerization versus hydrogenation. We show that complexes initially present as Rh(C<sub>2</sub>H<sub>4</sub>)<sub>2</sub> bonded to the zeolite catalyze both the dimerization and hydrogenation of ethene, with a high selectivity for the former, and that treatment of the catalyst to make rhodium clusters of only a few atoms each, on average, boosts the activity for hydrogenation and essentially eliminates that for dimerization. Moreover, these changes are reversible.

Spectra of the working catalyst demonstrate the structural changes that determine the selectivity, which occur at the very early stages of cluster formation and breakup. The data also demonstrate unprecedented performance of the site-isolated rhodium complexes, as rhodium complexes in the absence of labile ligands such as halides have been regarded as inactive for C–C bond formation.<sup>12–14</sup> We infer from our results that both rhodium in the form of mononuclear species and the acidic zeolite support are essential for catalysis of the dimerization reaction.

The structurally well-defined supported rhodium complex precursor was synthesized as before<sup>15</sup> by reaction of Rh(C<sub>2</sub>H<sub>4</sub>)<sub>2</sub>-(acac) (acac = acetylacetonate) with dealuminated HY zeolite (Si/Al atom ratio = 30), leading to nearly uniform rhodium

diene complexes anchored to the zeolite at acidic aluminum sites. The structure was determined by IR and extended X-ray absorption fine structure (EXAFS) spectra, which showed that the rhodium complex incorporating two ethene ligands  $\pi$ -bonded to Rh (with a Rh–C coordination number of nearly 4) is linked to the zeolite by two Rh–O bonds [Table S1 and Figure S1 in the Supporting Information (SI)]. The IR results indicate that 20–25% of the protons initially present on the zeolite are exchanged for the rhodium complexes in the synthesis (Figure S2). No evidence of the formation of rhodium hydride species was found (Figure S3).

When the catalyst was treated with flowing H<sub>2</sub> for 1.5 h at 1 bar and room temperature, rhodium clusters formed, as expected.<sup>16</sup> The Rh–Rh coordination number determined by EXAFS spectroscopy was 1.9 (Table S1), showing an average nuclearity of less than  $\sim 3$  and thus the presence of extremely small clusters along with unconverted mononuclear rhodium species. The cluster formation led to only a small decrease in the Rh–O and Rh–Al coordination numbers, consistent with the smallness of the clusters (Table S2). Thus, the data indicate a minimal alteration of the metal–support bonding as a result of cluster formation.

The catalytic behavior of each of the variously treated samples was evaluated for the conversion of ethene in the presence of H<sub>2</sub> in a once-through plug-flow reactor at atmospheric pressure and 303 K. The gas-phase products were monitored as a function of time on stream with an online gas chromatograph. To provide quantitative determinations of the catalytic activity, experiments were done with the reactor operating with conversions in the differential range (<10%, Figure S2), allowing the direct determination of reaction rates expressed as turnover frequencies (TOFs) (Table 1). For each form of the catalyst, total numbers of turnovers exceeding 1500 could always be attained within 4–10 h on stream, clearly demonstrating that the transformations are catalytic.<sup>17</sup>

In ethene-rich mixtures (C<sub>2</sub>H<sub>4</sub>/H<sub>2</sub> molar ratio = 4), the catalysts after each pretreatment were found to be active and highly selective for ethene dimerization (Table 1); ethene hydrogenation was only a minor side reaction.<sup>18</sup> This result is surprising, as the activities of rhodium catalysts for formation of C–C bonds are usually observed only when activating ligands such as halides are bonded to the rhodium<sup>12–14</sup> and the selectivity for butenes characterizing other supported catalysts,

**Received:** December 30, 2010

**Published:** March 10, 2011

**Table 1. Performance in a Once-Through Plug-Flow Reactor of the Catalyst Formed by Adsorption Of  $\text{Rh}(\text{C}_2\text{H}_4)_2(\text{acac})$  on Dealuminated Zeolite HY<sup>a</sup>**

catalyst pretreatment	feed composition ( $\text{C}_2\text{H}_4/\text{H}_2$ molar ratio)	TOF ( $\text{s}^{-1}$ ) <sup>d</sup>	selectivity (mol %) <sup>e,f</sup>		
			ethane	butenes	butane
none <sup>b</sup>	4.00	0.075	18.9	78.2	1.9
none <sup>b</sup>	0.25	0.260	22.0	72.5	4.5
$\text{H}_2$ <sup>c</sup>	4.00	0.071	20.4	76.5	3.1
$\text{H}_2$ <sup>c</sup>	0.25	0.932	89.3	7.6	3.1

<sup>a</sup> Reaction conditions: once-through flow reactor operated at 303 K and 1 bar ( $\text{C}_2\text{H}_4$  and  $\text{H}_2$  were present with helium at a partial pressure of 0.5 bar).

<sup>b</sup> Catalyst used as prepared. <sup>c</sup> Flowing  $\text{H}_2$  at 303 K and 1 bar for 1.5 h prior to use. <sup>d</sup> Turnover frequencies calculated from differential conversions (by extrapolation to time = 0) assuming that all of the Rh atoms were accessible to the reactants. <sup>e</sup> Selectivities were independent of conversion within the range investigated (0.5–12%). <sup>f</sup> As a secondary product, butane was invariably formed in low yields at the low observed conversions.

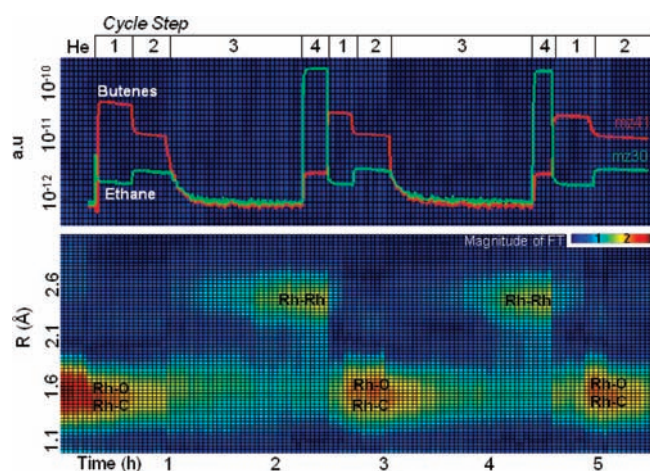


**Figure 1.** (top) Changes in selectivity of the supported catalyst initially containing  $\text{Rh}(\text{C}_2\text{H}_4)_2$  supported on HY zeolite and (bottom) catalyst structure represented by the Fourier transform function determined from time-resolved EXAFS data as a function of the composition of the feed (shown as molar ratios), which was cycled in the following sequence: (1) 4:1:5  $\text{C}_2\text{H}_4/\text{H}_2/\text{He}$ ; (2) 1:4:5  $\text{C}_2\text{H}_4/\text{H}_2/\text{He}$ ; (3) pure  $\text{H}_2$ ; (4) 1:4:5  $\text{C}_2\text{H}_4/\text{H}_2/\text{He}$ . In the bottom panel, the horizontal axis represents time on stream, the vertical axis the Rh–backscatterer distance (not corrected for phase shifts), and the colors the magnitudes of various contributions (related to the abundance of backscatterer atoms at a particular Rh–backscatterer distance; a change in color from red to yellow to green to blue shows a continuing decrease in intensity of the contribution). The peak at  $\sim 2.5$  Å includes the Rh–Rh contribution together with Rh–Al and Rh– $\text{C}_{\text{long}}$  contributions (comparatively much less intense), and the peak at  $\sim 1.6$  Å includes the Rh–low-Z-scatterer contributions, Rh–O and Rh–C. Details of the EXAFS data fitting are provided in Table S1. The experiment was carried out in an EXAFS cell/flow reactor at 303 K and 1 bar.

such as reduced cobalt oxides,<sup>19</sup> nickel oxides,<sup>20</sup> and ruthenium clusters,<sup>21</sup> in the presence of  $\text{H}_2$  rarely exceeds 1%.

In contrast, when the feed stream was  $\text{H}_2$ -rich ( $\text{C}_2\text{H}_4/\text{H}_2$  molar ratio = 0.25), markedly different product distributions were observed for the two pretreatments of the catalyst (Table 1). The sample initially incorporating rhodium clusters (along with rhodium complexes) was highly active and selective for hydrogenation, in contrast to the catalyst containing the rhodium complexes without clusters, which was selective for dimerization. Moreover, the rate of dimerization on the rhodium

complexes was boosted by an increase in the  $\text{H}_2$  partial pressure (Figure S6), with only a moderate accompanying decrease in the selectivity for butenes (from  $\sim 78\%$  with a  $\text{C}_2\text{H}_4/\text{H}_2$  molar ratio of 4 to  $\sim 72\%$  with a  $\text{C}_2\text{H}_4/\text{H}_2$  molar ratio of 0.25).<sup>22</sup>

Complementary experiments were carried out to characterize the working catalyst in an EXAFS cell serving as a flow reactor (an integral reactor, not a differential one). To identify the catalytically active rhodium species, we recorded spectra at the rhodium K edge characterizing dynamic changes in the catalyst structure after step changes in the feed  $\text{C}_2\text{H}_4/\text{H}_2$  ratio. The X-ray beam was focused right at the inlet of the flow reactor/cell<sup>23</sup> to provide data representing the catalyst in an atmosphere essentially matching that of the feed (and that throughout the differential plug-flow reactor). EXAFS spectra were recorded at 3 min intervals during the experiment, and the composition of the product from this integral flow reactor was determined periodically by mass spectrometry. The composition of the feed stream was cycled in the following sequence: (1)  $\text{C}_2\text{H}_4$ -rich; (2)  $\text{H}_2$ -rich; (3) pure  $\text{H}_2$ ; and (4)  $\text{H}_2$ -rich. Specifics are given in the caption of Figure 1, which includes a summary of the time-resolved EXAFS and mass spectrometric data recorded over several cycles.

Fourier-transformed  $k^3$ -weighted EXAFS data<sup>24</sup> are shown in the bottom panel of Figure 1 as a function of time on stream for the consecutive feed cycles (for details, see the figure caption). The data show the evolution of the magnitude of the EXAFS function (colored areas in the diagram) for Rh–backscatterer contributions at short distances ( $\sim 1.6$  Å, not phase-shift-corrected) assigned to Rh–O and Rh–C together with the longer-distance contribution ( $\sim 2.5$  Å, not phase-shift-corrected) ascribed to Rh–Rh, Rh–Al, and Rh– $\text{C}_{\text{long}}$ .<sup>15</sup> For each step in the cycle, changes in the magnitude of the Fourier transform for each contribution were observed (Figure 1), indicating changes in the structure/ligation of the Rh atoms in the catalytic sites, as explained below. The catalyst selectivity data (represented by fragments at  $m/z$  30 and 41 corresponding to ethane and butenes, respectively, in the effluent), which are plotted above the EXAFS results in Figure 1, are clearly correlated with changes in the catalyst structure (these selectivity data determined with the integral reactor only approximately match those obtained with the differential reactor).<sup>25</sup> More detailed structural information provided by the EXAFS results is given in Figure S8 and Table S1; details of the data fitting are given in the SI.

The results in Figure 1 show that when the ethene-rich mixture initially flowed through the bed of catalyst containing

the mononuclear rhodium complexes (cycle step 1), *n*-butenes were the major catalytic reaction products. The data measured in the differential reactor determined the rates of formation of *n*-butenes and ethane to be 0.059 and 0.014 s<sup>-1</sup>, respectively (corresponding to a total TOF of 0.075 s<sup>-1</sup>; Table 1, entry 1). Under these conditions, the mononuclear rhodium complexes were stable, with no Rh–Rh contributions (no clusters) detected by EXAFS spectroscopy, although a decrease in the Rh–light-scatterer contribution was observed with increasing time on stream (Figure 1 and Figure S8), indicating a change in the ligation of the rhodium (for details, see Table S1). Specifically, the EXAFS data (Figure S8) indicate that during the selective dimerization reaction, each Rh atom was, on average, bonded to only 2.5 C atoms, consistent with the inference that a fraction of the initially present  $\pi$ -bonded ethene ligands were converted to reaction intermediates such as alkyls. Correspondingly, a weak contribution (identified as a second Rh–C shell) was observed at a distance longer than a bonding distance (Table S1), as expected for butyl ligands formed on the rhodium sites during the dimerization reaction. The formation of oligomeric intermediates on the surface of the catalyst was also evidenced by the IR spectra, which showed conversion of the ethene ligands initially  $\pi$ -bonded to the rhodium sites (bands at 3084, 3060, and 3016 cm<sup>-1</sup>) and the appearance of new bands at 2875, 2935, and 2960 cm<sup>-1</sup> as a result of the dimerization reaction (see Figure S8 for details).

When the H<sub>2</sub>/ethene partial pressure ratio was subsequently increased to 4 (cycle step 2; Table 1, entry 2), the catalyst was still selective for *n*-butene formation, but the yields of the hydrogenation products ethane and butane (a secondary product, not shown in the plot) increased. Within the error of the EXAFS data, there was no evidence of rhodium species other than mononuclear complexes during this phase of the experiment, which indicates that the presence of ethene in the gas phase, even at low concentrations, stabilizes these mononuclear species, being a continuous source of ligands to maintain the rhodium nuclearity. However, a further decrease observed in the ratio of the short to long Rh–C contributions (Table S2) suggests a higher conversion of the adsorbed ethene ligands into reaction intermediates such as butyl (or ethyl), corresponding to the higher H<sub>2</sub> partial pressure.

In the next phase of the experiment (cycle step 3), the feed was switched to pure H<sub>2</sub>, with the catalyst still incorporating the mononuclear rhodium species. During the next 1.5 h, a Rh–Rh contribution gradually grew in (Figure 1) and reached a final coordination number of 1.9 (Figure S9), indicating the formation of clusters. Concomitantly, the Rh–C, Rh–Al, and Rh–O contributions decreased slightly (Figure S8 and Table S1). After the H<sub>2</sub> treatment, the feed was switched to an H<sub>2</sub>-rich mixture (H<sub>2</sub>/ethene molar ratio = 4). The rhodium clusters were then stable and highly active catalytically, and the selectivity for hydrogenation was high (Figure 1, corresponding to Table 1, entry 4). Under these conditions, the stability of the rhodium clusters in the working state corresponds to the presence of H<sub>2</sub> in large excess, and any ethene present is rapidly converted on the clusters.

A comparison of the rates of dimerization and hydrogenation during catalysis in the H<sub>2</sub>-rich mixture before and after cluster formation indicated a dramatic increase in the rate of hydrogenation upon formation of clusters: the ethane formation rate increased from 0.057 s<sup>-1</sup> with only complexes to 0.83 s<sup>-1</sup> when clusters were present.

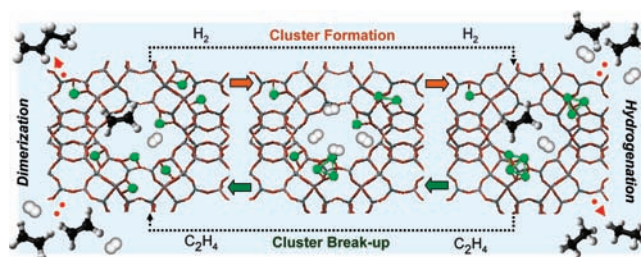


**Figure 2.** Simplified schematic representation of the state of the rhodium (green) in the catalyst attained at each step in the cycle, as the catalytic performance of the solid is tuned.

A subsequent increase of the C<sub>2</sub>H<sub>4</sub>/H<sub>2</sub> molar ratio to 4 (making H<sub>2</sub> the limiting reactant) led to the rapid breakup of the rhodium clusters by oxidative fragmentation by ethene,<sup>26</sup> as indicated by the disappearance of the Rh–Rh contribution (Figure 1), accompanied by a sharp drop in the rate of hydrogenation and a concomitant increase in the rate of *n*-butene formation. The rate of ethane formation declined from 0.83 to 0.057 s<sup>-1</sup>, and the rate of dimer formation increased from 0.071 to 0.19 s<sup>-1</sup>, corresponding to a marked increase in the selectivity for dimerization over hydrogenation, with the ratio of the butene and ethane formation rates increasing 40-fold.

The process described above was carried out through repeated cycles (Figure 1); the changes were reversible.

The EXAFS data demonstrate that in H<sub>2</sub>-rich reaction mixtures, both the rhodium complexes and the rhodium clusters are stable (no changes were observed in the rhodium nuclearity during the experiment); the complexes selectively produce *n*-butenes and the clusters selectively produce ethane (see cycle steps 2 and 4 in Figure 1, corresponding to entries 2 and 4 in Table 1). Thus, our data allow a quantification of the changes in the catalyst behavior at the very early stages of cluster formation, when only few Rh–Rh bonds had been formed and only a portion of the rhodium had been converted into clusters (Figure 2). When hydrogenation was the predominant reaction, it was so fast in comparison with dimerization that the latter was swamped. The data show that the clusters are highly active catalysts for C–H bond formation, much more active than the complexes.

The mononuclear Rh(I) species catalyze both hydrogenation and dimerization. The latter has been observed for halide-containing rhodium complexes,<sup>12,27</sup> but our new observation of such activity for the rhodium complex on the halide-free zeolite indicates an important role of the acidic support in the formation of C–C bonds. We emphasize that the precursor of our supported catalyst, Rh(C<sub>2</sub>H<sub>4</sub>)<sub>2</sub>(acac), itself does not catalyze ethene dimerization.<sup>12</sup> Indeed, chemisorption of this precursor on highly dehydroxylated MgO led to supported Rh(C<sub>2</sub>H<sub>4</sub>)<sub>2</sub> species that were isostructural to those in the zeolite-supported rhodium complexes (Table S3) but shown by our data to be inactive for the formation of butenes, being 100% selective for hydrogenation in the presence of H<sub>2</sub>.

The results of blank experiments confirmed that the zeolite alone did not provide the catalytic activity for dimer formation at the temperature of our experiments (with or without H<sub>2</sub> co-fed with the alkene). Formation of C–C bonds on the zeolite started only when the temperature was increased to 433 K, consistent with previous reports,<sup>28,29</sup> and even then the dimer yield was 2 orders of magnitude less than with the zeolite-supported rhodium complexes operating at room temperature.<sup>30</sup>

In summary, our acidic zeolite-supported rhodium complex catalyst is active for dimerization in the absence of halides and selective for this reaction in a reducing atmosphere of H<sub>2</sub> (although the expected hydrogenation of the C=C bond occurs as an accompanying reaction; Table 1). On the basis of our results, we infer an important role of the zeolite as a macroligand of the rhodium complexes, altering the electron density on the rhodium or opening the possibility for cooperation between the rhodium complexes and the acidic Al—OH sites of the zeolite.<sup>31</sup> Further, the results demonstrate how regulation of the structure of the active sites of a supported catalyst at the molecular level (switching between rhodium complexes and rhodium clusters) allows fine-tuning of the catalyst selectivity simply by variation of the feed composition. To our knowledge, this is the first example of precise control of the selectivity of a solid catalyst by tuning of the structure of essentially molecular supported species.

## ■ ASSOCIATED CONTENT

**S Supporting Information.** Experimental procedures, synthesis of catalysts, reactivity tests, and details of the EXAFS fitting. This material is available free of charge via the Internet at <http://pubs.acs.org>.

## ■ AUTHOR INFORMATION

### Corresponding Author

bcgates@ucdavis.edu

## ■ ACKNOWLEDGMENT

We thank DOE (Basic Energy Sciences, Contract FG02-87ER15600) for support and acknowledge beam time and support of the DOE Division of Materials Sciences for its role in the operation and development of beamline MR-CAT at the Advanced Photon Source at Argonne National Laboratory.

## ■ REFERENCES

- (1) Lee, I.; Delbecq, F.; Morales, R.; Albiter, M. A.; Zaera, F. *Nat. Mater.* **2009**, *8*, 132.
- (2) Bell, A. T. *Science* **2003**, *299*, 1688.
- (3) Fujidala, K. L.; Tilley, T. D. *J. Catal.* **2003**, *216*, 265.
- (4) DeVos, D. E.; Dams, M.; Sels, B. F.; Jacobs, P. A. *Chem. Rev.* **2002**, *102*, 3615.
- (5) Thomas, J. M. *Top. Catal.* **2001**, *15*, 85.
- (6) Xu, Z.; Xiao, F.-S.; Purnell, S. K.; Alexeev, O.; Kawi, S.; Deutsch, S. E.; Gates, B. C. *Nature* **2002**, *372*, 346.
- (7) Corker, J.; Lefebvre, F.; Evans, J.; Lécuyer, C.; Dufaud, V.; Quignard, F.; Choplin, A.; Basset, J.-M. *Science* **1996**, *271*, 966.
- (8) Fujidala, K. L.; Drake, I. J.; Bell, A. T.; Tilley, T. D. *J. Am. Chem. Soc.* **2004**, *126*, 10864.
- (9) Alacon, M. J.; Corma, A.; Iglesias, M.; Sanchez, F. *J. Organomet. Chem.* **2002**, *655*, 134.
- (10) Sachtler, W. M. H.; Zhang, Z. *Adv. Catal.* **1993**, *39*, 129.
- (11) Stakheev, A. Yu.; Kustov, L. M. *Appl. Catal., A* **1999**, *188*, 3.
- (12) Cramer, R. *J. Am. Chem. Soc.* **1965**, *87*, 4717.
- (13) Alderson, T.; Jenner, E. L.; Lindsey, R. V. *J. Am. Chem. Soc.* **1965**, *87*, 5638.
- (14) Fagnou, K.; Lautens, M. *Chem. Rev.* **2003**, *103*, 169.
- (15) Liang, A. J.; Bhirud, V. A.; Ehresmann, J. O.; Kletnieks, P. W.; Haw, J. F.; Gates, B. C. *J. Phys. Chem. B* **2005**, *109*, 24236.
- (16) Liang, A. J.; Gates, B. C. *J. Phys. Chem. C* **2008**, *112*, 18039.

(17) Deactivation of the catalyst was observed, as shown in Figure S5, and we infer that it was caused by the formation of oligomers that adsorb strongly on the catalytically active species.

(18) As demonstrated later in the manuscript, the similar catalytic performance of reduced and unreduced catalysts in flowing ethene-rich mixtures (Table 1, entries 3 and 1, respectively) arises because the rhodium clusters initially present in the former break up upon contact with the feed, so both classes of samples are characterized by the presence of mononuclear rhodium complexes under working conditions.

(19) Kokes, R. J. *J. Catal.* **1969**, *14*, 83.

(20) Kokes, R. J.; Bartek, J. P. *J. Catal.* **1968**, *12*, 72.

(21) Rodriguez, E.; Leconte, M.; Basset, J.-M.; Tanaka, K. *J. Catal.* **1989**, *119*, 230.

(22) The role of H<sub>2</sub> in dimerization reactions has often been ascribed to the generation (or regeneration) of metal hydride species that facilitate the activation of the alkene or the desorption of dimeric intermediates. For a comprehensive review, see: Pillai, S. M.; Ravindranathan, M.; Sivaram, S. *Chem. Rev.* **1986**, *86*, 353.

(23) Odzak, J. F.; Argo, A. M.; Lai, F. S.; Gates, B. C.; Pandya, K.; Feraria, L. *Rev. Sci. Instrum.* **2001**, *72*, 3943.

(24) Koningsberger, D. C.; Mojet, B. L.; van Dorssen, G. E.; Ramaker, D. E. *Top. Catal.* **2000**, *10*, 143.

(25) Some differences in the distribution of reaction products shown in Table 1 and Figure 1 were expected, as the EXAFS cell used as a reactor to collect the data of Figure 1 could not be operated in the differential conversion range because of the limitation that relatively large masses of catalyst had to be used to optimize the quality of the EXAFS data.

(26) Oxidative fragmentation of small metal clusters by ethene in solution has been demonstrated. See: (a) Adams, C. J.; Bruce, M. I.; Liddell, M. J.; Tiekink, E. R. T.; Skelton, B. W.; White, A. H. *J. Organomet. Chem.* **1993**, *445*, 187. (b) Kampe, C. E.; Boag, N. M.; Kaesz, H. D. *J. Mol. Catal.* **1983**, *21*, 297. More recently, it has also been demonstrated on solid surfaces. See: (c) Uzun, A.; Gates, B. C. *Angew. Chem., Int. Ed.* **2008**, *47*, 9245. The mechanism of this transformation remains uncharacterized. On the basis of the changes that we determined by EXAFS spectroscopy upon breakup of the rhodium clusters, the following approximate stoichiometry is tentatively proposed: Rh<sub>3</sub>-(C<sub>2</sub>H<sub>5</sub>)<sub>3</sub> + 3C<sub>2</sub>H<sub>4</sub> + 1.5H<sub>2</sub> → 3Rh(C<sub>2</sub>H<sub>5</sub>)<sub>2</sub>. We emphasize the approximate nature of this statement, as EXAFS spectroscopy provides only average information about the structure of the rhodium sites.

(27) Takahashi, N.; Okura, I.; Keii, T. *J. Am. Chem. Soc.* **1975**, *97*, 7489.

(28) Derouane, E. G.; Gilson, J.-P.; Nagy, J. B. *J. Mol. Catal.* **1981**, *10*, 331.

(29) Cant, N. W. F.; Hall, W. K. *J. Catal.* **1972**, *25*, 161.

(30) Poisoning of the anchored rhodium complexes with small amounts of CO, leading to the formation of anchored rhodium gem-dicarbonyl [Rh(CO)<sub>2</sub>] species as shown by IR spectroscopy (Figure S1), led to complete deactivation of the zeolite-supported catalyst, consistent with the inference that the rhodium species participate in the C—C bond formation reaction (the interaction of CO with the acidic sites of the zeolite is very weak at 303 K, as evidenced by the result that the intensities of the IR bands characterizing the acidic —OH groups at 3630 and 3535 cm<sup>-1</sup> did not decrease upon contact of the sample with CO).

(31) Sachtler, W. M. H.; Stakheev, A. Yu. *Catal. Today* **1992**, *12*, 283.